Rare Metal Materials and Engineering
Volume 50, Issue 10, October 2021
Available online at www.rmme.ac.cn

Science Press

Cite this article as: Liu Shichao, Lei Pengfei, Liu Min, et al. Additive Manufactured Ti-6Al-4V Alloy with Graded Microstructure by Selective Laser Melting[J]. Rare Metal Materials and Engineering, 2021, 50(10): 3543-3549.

ARTICLE

Additive Manufactured Ti-6Al-4V Alloy with Graded Microstructure by Selective Laser Melting

Liu Shichao[1,2], Lei Pengfei[3], Liu Min[1,2], Zhang Gengming[1,2], Chen Chao[1,2], Zhou Kechao[1,2]

[1] Powder Metallurgy Research Institute, Central South University, Changsha 410083, China; [2] State Key Laboratory of Powder Metallurgy, Central South University, Changsha 410083, China; [3] Department of Orthopaedics, Xiangya Hospital, Central South University, Changsha 410083, China

Abstract: Graded Ti-6Al-4V alloys were produced by selective laser melting (SLM). Regulation of laser power and scanning speed was applied separately on each sample along the building direction. The microstructure transformation and phase transition in the graded Ti-6Al-4V were investigated. Results show that due to the rapid cooling rate of the SLM process, the microstructure of Ti-6Al-4V is mainly acicular α' martensite in prior β column grains. The β column grains are enlarged with the increase of laser power or the decrease of scanning speed. The preferential orientation of α' grains changes due to the variation of laser power and scanning speed. Moreover, the ascending scanning speed or descending scanning speed during the process may lead to two different defects.

Key words: additive manufacturing; selective laser melting; Ti-6Al-4V; graded microstructure; columnar grain

Additive manufacturing is a technique that combines computer-aided design and material processing and forming technology. Components can be built up layer by layer according to the three-dimensional model data. The technique increases the flexibility of design and manufacturing, which allows to fabricate near-net-shape parts rapidly with complex geometries.

For additive manufacturing of metallic parts, selective laser melting (SLM) is a commonly applied technique that uses metallic powders as stocks. Firstly, the quality of metallic powders is important to the SLM made products. According to the previous study[1], spherical metallic powders are more likely to fabricate parts with fewer defects. Suitable process parameters (e. g. laser power, scan speed, hatch space, layer thickness) also need to be considered to make qualified products. Otherwise, the inappropriate process parameters which indicates unbalanced energy will lead to defects like porosity, delamination between layers, balling effect and hot tears[2]. Therefore, lots of works have been done to search the appropriate process parameters for the corresponding materials. Take Ti-6Al-4V for example, the influence of different process parameters and scanning strategy on the microstructure and mechanical properties of SLM Ti-6Al-4V was studied, and optimum combinations of laser power, scanning velocity, hatch spacing, layer thickness and scanning rotation were suggested[3,4]. SLM generally create a unique columnar microstructure with different kinds of metallic materials like Ti alloys, Ni alloys, etc[5-8]. Because there is no nucleation barrier to solidification during the process, the grains will grow epitaxially[4]. Columnar microstructure will cause anisotropy of mechanical properties, especially fatigue performances[9]. However, Murr[10], Niendorf[11] and Thijs[12] et al have attempted to obtain products with controllable texture by adjusting the process parameters. According to these studies, either highly anisotropic microstructure or equiaxed fine-grained microstructure can be obtained using the corresponding scanning strategies. Besides the adjustment of the process parameters, another method to achieve the equiaxed fine-grained microstructure is to pre-functionalize the metallic powders with nanoparticles[13]. This method can help grain refinement by introducing new nucleation caused by nanoparticles. In our research group,

Received date: October 11, 2020
Foundation item: National Key R&D Program of China (2018YFB0704100); Key-Area Research and Development Program of Guangdong Province (2019B010943001); Natural Science Foundation of Hunan Province (2018JJ3654); Fund of State Key Laboratory of Powder Metallurgy, Central South University; International Exchange Program of China Postdoctoral Science Foundation
Corresponding author: Chen Chao, Ph. D., Professor, State Key Laboratory of Powder Metallurgy, Central South University, Changsha 410083, P. R. China, E-mail: pkhqchenchao@126.com

both of the methods have been tried to control the microstructure of Ti alloys[14,15].

By taking one step further, rather than fabricating a component with a single uniform microstructure, functional gradient parts processed by SLM were explored. The transitions of the texture, microstructure and mechanical properties of Inconel 718 and 316L stainless steel with various process parameters were demonstrated[16,17]. These studies help to develop process strategy to design functional graded components with tailored properties. Ti alloys, as one of the commonly used materials in aerospace industry, can be applied to many parts like engine and fuselage. Since the parts in engine work under complicate environment and complex force conditions, anisotropy is not a complete disadvantage to some extent. Some regions need column microstructure to improve creep resistance, while other areas may require a higher hardness achieved by equiaxed fine-grained microstructure. Hence, it will be attractive to develop functional gradient parts of Ti alloys to satisfy various requirements for applications.

In this study, several graded Ti-6Al-4V parts were produced by regulating parameters in the SLM process. The laser power or scanning speed were changed gradually along the building direction. The microstructure transformation and phase transition of the whole sample were examined. The morphology and size of β grains and α/α' phase in the graded parts were illustrated. The capability of microstructure control of SLM Ti-6Al-4V within one single block only by process parameter adjustment was checked.

1 Experiment

Ti-6Al-4V pre-alloyed powders were used in the study. Table 1 shows the chemical composition of the powder. The powder has a good sphericity with a particle diameter ranging from d_{10}=16 μm to d_{90}=56 μm. The spherical morphology of the powder is shown in Fig.1.

Table 1 Chemical composition of Ti-6Al-4V powder (wt%)

Al	V	Fe	O	N	H	Ti
5.87	3.22	0.096	0.0087	0.015	0.009	Bal.

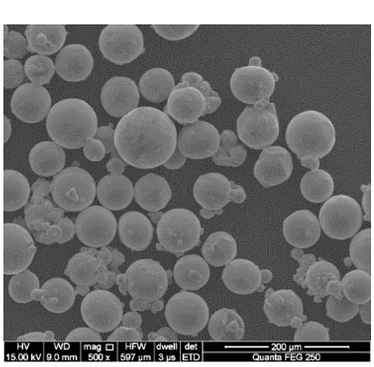

Fig.1 SEM morphology of Ti-6Al-4V powder

Two batches of samples were built in Farsoon 271M SLM system. The first batch was laser power graded blocks of 10 mm×10 mm×6.5 mm. The laser power increased or decreased as the height went up. In order to build up the samples successfully and eliminate the potential bonding problems between the sample and the substrate, a 1 mm thick layer was deposited using the laser power of 100 W and the scanning speed of 1000 mm/s firstly. And then the laser power was gradually changed every 0.9 mm from 100 W to 480 W, while the scanning speed was fixed at 1000 mm/min. The other batch of the samples were scanning speed graded blocks, and the scanning speed increased or decreased as the height went up. It had a 1 mm foundation deposited using the laser power of 200 W and the scanning speed of 1000 mm/s. The scanning speed would start to change every 0.9 mm from 200 mm/s to 1800 mm/s. The details of the process parameters of these two batches are listed in Table 2 and Table 3. The hatch space and layer thickness were set as 0.12 and 0.03 mm, respectively according to the literature and previous works[4,14]. Fig. 2 shows how the graded samples finally appear as the process parameters change.

The graded samples were cut along the *xz*-plane, and etched by the Kroll's reagent after grinding and polishing. The microstructure was examined by a Leica DM2700P optical microscope and Tescan Mira 3 scanning electron microscope (SEM) equipped with energy-dispersive spectroscopy (EDS). The electron backscattered diffraction (EBSD) analysis was performed using SEM at accelerating voltage of 20 kV and

Table 2 Gradient setting of laser power at a scanning speed of 1000 mm/s, hatch space of 0.12 mm, and layer thickness of 0.03 mm

Sample P1		Sample P2	
Height/mm	Laser power/W	Height/mm	Laser power/W
0~1.9	100	0~1	100
1.9~2.8	200	1~1.9	480
2.8~3.7	300	1.9~2.8	400
3.7~4.6	400	2.8~3.7	300
4.6~5.5	480	3.7~4.6	200
		4.6~5.5	100

Table 3 Gradient setting of scanning speed at a laser power of 200 W, hatch space of 0.12 mm, and layer thickness of 0.03 mm

Sample S1		Sample S2	
Height/ mm	Scanning speed/ $mm \cdot s^{-1}$	Height/ mm	Scanning speed/ $mm \cdot s^{-1}$
0~1	1000	0~1	1000
1~1.9	200	1~1.9	1800
1.9~2.8	600	1.9~2.8	1400
2.8~3.7	1000	2.8~3.7	1000
3.7~4.6	1400	3.7~4.6	600
4.6-5.5	1800	4.6~5.5	200

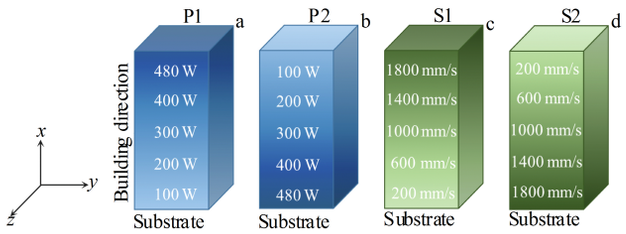

Fig.2 Schematics of the laser power graded (a, b) and scanning speed graded (c, d) Ti-6Al-4V samples (only gradient layers are shown in the figure; for all the four samples, a 1 mm base layer has been deposited on the substrate using 100 W (for P1 and P2) or 200 W (for S1 and S2) laser power and 1000 mm/s scanning speed to guarantee the combination between the substrate samples and insure that the building-up can be proceeded successfully)

with a step size of 0.6 μm.

XRD patterns were obtained by X-ray diffraction (Brukers D8 Advance). The diffraction patterns were recorded within the 2θ range of 10°~100° with a step size of 0.02°. Vickers hardness measurements were taken on the graded samples under 4.9 N (denoted as HV0.5). A 3×15 matrix of the hardness test points has been taken on the graded samples, a small 3×3 matrix was guaranteed to be measured in each process parameter section. The distance between each point was 0.3 mm.

2 Results and Discussion

2.1 Microstructures of laser power graded alloys

Fig. 3 shows OM images of the whole graded sample P1 from the bottom (100 W) to the top (480 W). As can be seen, 100 W part has a porosity of around 11.26% due to the lack of energy. As the laser power goes up to 200 W, the sample begins to be fully dense. It starts with a fine-grained microstructure and then an epitaxial growth of columnar dendrites occurs along the building direction due to the unique laser deposition technique [18]. Column grains and melting pool can be observed at the upper part of the sample. Fig.4a shows the prior columnar β grains in sample P1, of which the laser power increases as the height goes up. The width of column grains in 200 W section is 30~100 μm. The column grains get slightly larger as the laser power goes up. At 480 W, the average column grain width is 212 μm. However, according to Fig. 4b of sample P2, when the laser power decreases as the height goes up, the bottom 480 W has a column grain width of 50~200 μm, and the top 200 W region has a column grain width of 105 μm. The columnar grains will get coarser because of the decreasing cooling rate[19]. With more energy input, the cooling rate can be lower, which lead to coarser columnar prior β grains, as presented in samples P1 and P2. This can be explained by the Hunt's dendritic growth model, which calculated the relationship between primary dendrite arm spacing λ and solidification parameters. The equation is

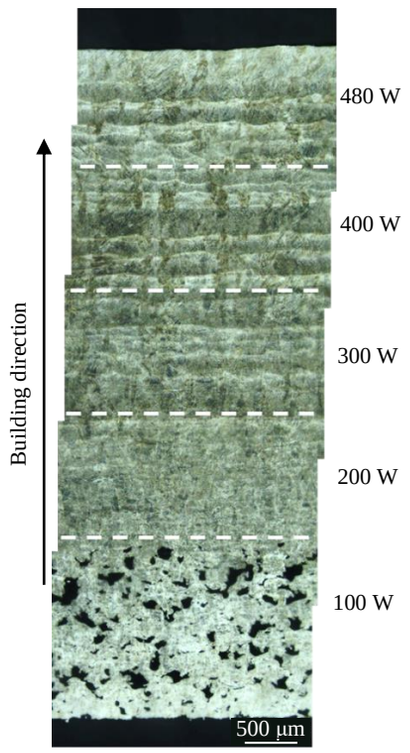

Fig.3 OM image of the laser power graded sample on *xz* plan

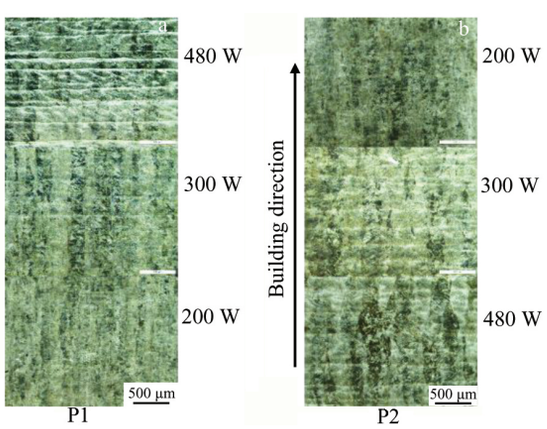

Fig.4 OM images of the laser power graded samples P1 (a) and P2 (b) (400 W area is not presented since it has a similar microstructure to 480 W area)

simplified and expressed as

$$\lambda=A(GV)^{-n} \quad (1)$$

where A and n are constants related to material, and $n>0$[20]; G is the temperature gradient and V is the solidification rate. With increasing the energy input, both G and V will decrease, thus leading to coarser dendrites according to the equation. The microstructure changes mildly and the boundaries between each laser power section are not distinguishable. Because during the SLM process, the deposited layer actually

goes through several re-melting and re-solidifying with neighboring layers and the change between each laser power is only 100 W. Therefore, the change of the thermal gradient and the cooling rate in the localized spot is not significant. Comparing P1 and P2 from the bottom to the top, the laser power that goes up or down based on the underlying layer makes not much differences as well. The retained energy below the melting pool is beneficial to the growth of grains, but the influence on the microstructure by altering the laser power within a small range is still quite restricted.

SEM images of the laser power graded samples are shown in Fig.5. There are not many differences between each sample and each laser power section. The microstructure of the graded samples is acicular martensitic phase in prior β columnar grains. In SLM, regarded as a fundamental localized solidification process, <001> solidification growth was reported to be parallel to the z-axis, which is the maximum thermal gradient for most cubic systems[2]. The formation of the β columnar grains can be influenced by temperature gradient and interface velocity. With a high temperature gradient and a relatively slow interface velocity, the grains are more likely to grow into cellular shape even planar rather than equiaxed dendritic grains [2]. Due to the high cooling rate caused by the high temperature gradients during the SLM process, the microstructure of SLM processed Ti-6Al-4V is martensitic [4]. According to the previous research work, the cooling rate of SLM process is generally within a range of 10^3~10^8 K/s which is much higher than the critical cooling rate of martensite transformation[21-26]. Prior β phase will transform into α' martensite, and the martensite microstructure does not change much from 200 W to 480 W. However, according to the XRD pattern shown in Fig.6, a few β phases are detected in 480 W part. With increasing the laser power, the extra energy retained can decompose some α' martensites into α and β phases [27]. Decomposed α phase is too small to be observed under SEM, while it is more likely to be found at the grain boundaries [28]. With the increase of the laser power, the intensity ratio of the diffraction peak (101) and (102) is changed gradually from 2.82 (200 W) to 0.38 (300 W), 0.20 (400 W) and 0.21 (480 W) eventually, which means that the preferential orientation of the α' grains changes from <101> to <102>. EBSD results in Fig. 7 clearly show the prior β columnar grains and the acicular α' martensite in it. The width of β column grains is 20~50 μm at 200 W and around 100 μm at 300 W. As for 480 W, the width of β columnar grains is above 100 μm.

2.2 Hardness variation of laser power graded alloys

The measured hardness is averaged and presented in Fig. 8. Despite 100 W area has a relatively low hardness of 3000 MPa because of its porous microstructure, the rest parts of the graded sample have a close hardness of 3800±200 MPa regardless of laser power. This is because the microstructures

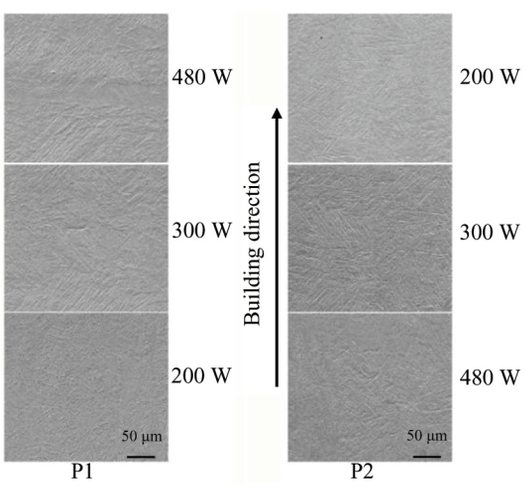

Fig.5 SEM images of the laser power graded samples P1 (a) and P2 (b)

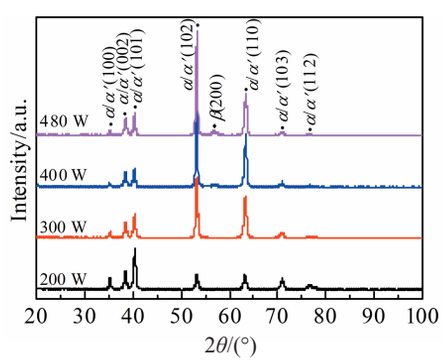

Fig.6 XRD patterns of the laser power graded sample P1

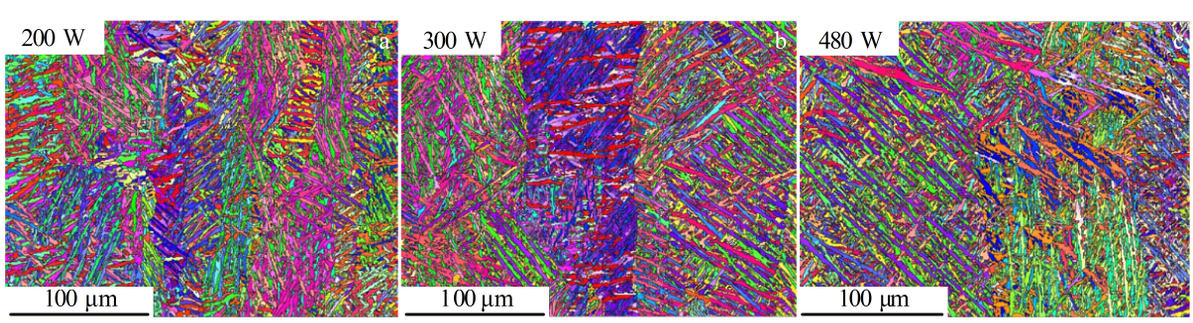

Fig.7 Inverse pole figures (IPF) of the laser power graded sample P1: (a) 200 W, (b) 300 W, and (c) 480 W

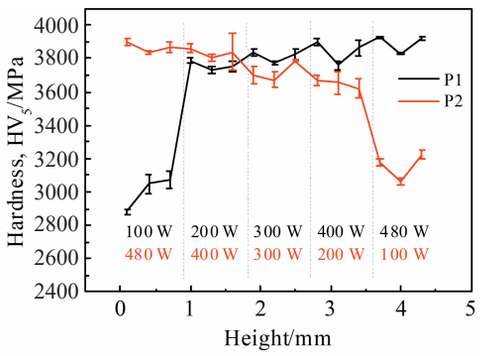

Fig.8 Hardness variation of laser power graded alloys from the bottom pre-deposited base layer (set as 0 mm) to the top layer

of the graded samples are all acicular α' martensite with similar sizes.

2.3 Microstructures of scanning speed graded alloys

Fig.9 and Fig.10 show optical microscope images and SEM images of scanning speed graded samples. For sample S1, despite of the base layers, the sample was deposited from 200 mm/s to 1800 mm/s. Sample S2 was deposited in the other way round, started with 1800 mm/s and decreased by 400 mm/s every 0.9 mm until 200 mm/s. The main microstructure of scanning speed graded samples is also acicular α' martensite in prior β columnar grains. In sample S1, the width of β columnar grains at 200 mm/s is 160~200 μm, and that of the grains at 600 and 1000 mm/s is about 100 and 60 μm respectively. When the scanning speed is raised up to 1400 mm/s, the columnar grains are obstructed by voids. As for sample S2, it starts with a microstructure full of defects when the scanning speed is 1800~1400 mm/s. The width of β column grains is about 65 μm when the scanning speed is 1000 mm/s. The grains grow to 70~150 μm when the scanning speed decreases to 600 mm/s. The width of β columnar grains can be as large as 250 μm as the scanning speed slows down to 200 mm/s. Generally, S2 has larger β columnar grains than S1 at the same scanning speed.

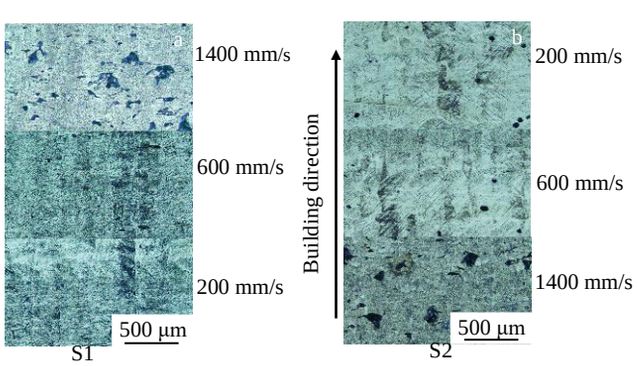

Fig.9 OM images of the scanning speed graded samples S1 (a) and S2 (b) (images of 1000 and 1800 mm/s are not demonstrated because they are similar to the morphology of 600 and 1400 mm/s, respectively)

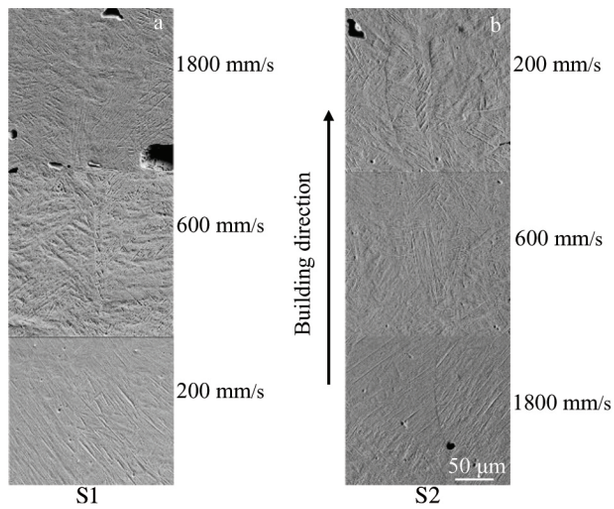

Fig.10 SEM images of the scanning speed graded samples S1 (a) and S2 (b) (images of 1000 and 1400 mm/s are not demonstrated because they are similar to the morphology of 600 and 1800 mm/s, respectively)

According to the XRD patterns in Fig. 11, there is no β phase remained when the scanning speed is between 600~1800 mm/s. When the scanning speed is as low as 200 mm/s, the sufficient energy allows the α' phase to partially decompose into $\alpha+\beta$ phases, so a small diffraction peak of β phase is found in the curve of 200 mm/s. When the scanning speed is between 200~600 mm/s, the preference of the α' grains orientation is <102>, and the intensity ratios of the diffraction peak of (101) and (102) are 0.55 and 0.18, respectively. As the scanning speed goes up to 1000~1800 mm/s, the preferential orientation of the α' grains changes to <101>, since the intensity ratio of the diffraction peak of (101) and (102) has increased to 1.57 (1000 mm/s), 5.99 (1400 mm/s) and 7.52 (1800 mm/s).

Compared to the laser power graded samples, scanning speed graded samples have two different kinds of voids, angular ones and sphere pores. The shape of the pores reveals the energy condition during the SLM process. When the pores are angular, it means that metal powder is not melted properly

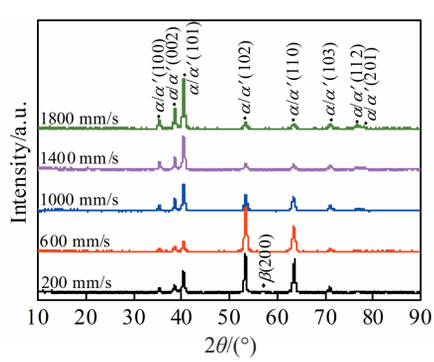

Fig.11 XRD patterns of the scanning speed graded sample S1

because of insufficient energy. On the other hand, if the energy density is too high, splashing may occur and bubbles may be trapped in the melting pool, which is the formation of sphere voids [29]. In sample S1, at the bottom 200 mm/s layers, it is fully dense without any voids. When the scanning speed is accelerated to 1400 mm/s, angular voids turn up. For sample S2, there are angular voids in 1800~1400 mm/s layers. As the scanning speed slows down, sphere pores appear on the top 200 mm/s layers.

Five layers at different scanning speeds are shown in Fig. 12, and the distribution of the voids in these layers is presented. Angular voids can be seen in layers of 1400~1800 mm/s, 1000 mm/s layer is pore-free, and sphere pores appear when the scanning speed goes down to 600 mm/s. Fig. 13a shows angular void in 1800 mm/s layer. It has irregular shape, and there are evenly unmelted Ti-6Al-4V powders in the hole. Fig. 13b shows sphere pores in 200 mm/s region, and the smooth surface can be seen inside the pores as like bubbles trapped in the block. The 200 mm/s layer in sample S2 has sphere pores in it, while the 200 mm/s layer in sample S1 is compact. Actually, the energy input is the same for the constant process parameters. The difference is caused by the distance to the substrate and the scanning speed for the previously deposited layers before changing, which indicates different degrees of energy loss. The 200 mm/s layer in S1 is at the bottom close to the substrate, and more heat can be conducted away to the substrate. The 200 mm/s layer in S2 is at the top and deposited on the 600 mm/s layer. Heat conduction is relatively restricted and more energy is retained in the melting pool, which leads to the sphere pores caused by the excessive energy in the local melting zone.

2.4 Hardness variation of scanning speed graded alloys

As can be seen in the hardness line chart (Fig. 14), 1400~1800 mm/s layers have a lower hardness of 3250±100 MPa than 3600±100 of 200~600 mm/s layers. The 1400~1800 mm/s layers deposited on 1000 mm/s layer have a relatively higher hardness than deposited layer near the substrate. The variation of hardness is due to the different porosity in each layer, which is related to their energy density as well.

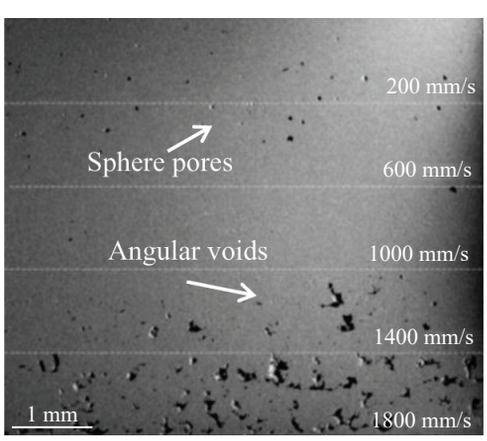

Fig.12 SEM image of scanning speed graded sample S2

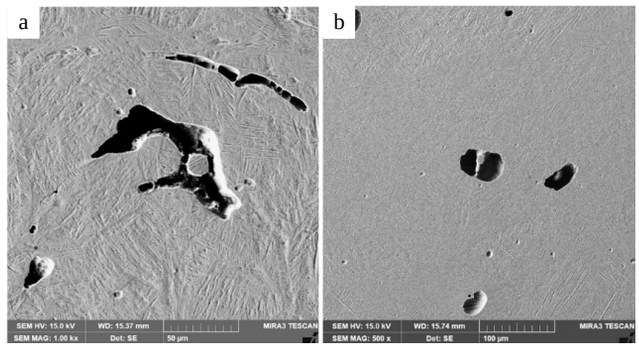

Fig.13 Two different voids in scanning speed graded sample: (a) 1800 mm/s and (b) 200 mm/s

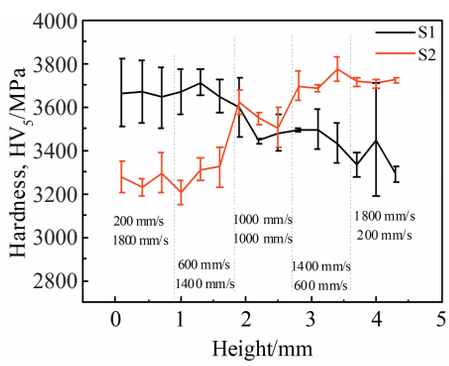

Fig.14 Hardness variation of scanning speed graded alloys (the height is set as 0 mm from the pre-deposited base layer, which means that the measurement starts from the bottom of the gradient part)

3 Conclusions

1) The changes of microstructure and mechanical properties of graded Ti-6Al-4V processed by SLM do not significantly depend on the gradually varying process parameters.

2) Because of the high cooling rate during SLM process, the microstructure of Ti-6Al-4V is acicular α' martensite in prior β column grains. The size of β columnar grains can be influenced by laser power and scanning speed, while the change of the microstructure does not have much effect on the hardness performance.

3) The hardness of SLMed Ti-6Al-4V is about 3800 MPa. As laser power increases from 200 W to 480 W (the scanning speed is kept as 1000 mm/s), the width of β column grains becomes larger from 30 μm to 200 μm. The width of β column grains changes from 60 μm to 250 μm when the scanning speed varies from 1000 mm/s to 200 mm/s (the laser power is 200 W). The more energy input in the melting pool and more heat retained in sub-deposited layers, the coarser the columnar grains tend to form.

4) Variation trending of scanning speed can affect the formation of defects. Slow scanning speed introduces too much energy into the melting pool. If it is deposited on the substrate or above high scanning speed layers, the sphere

pores is more likely to be eliminated due to a better heat conduction.

References

1 Zi Xuhui, Chen Chao, Wang Xiaojun *et al*. *Materials Science & Technology*[J], 2018, 34(6): 735

2 Collins P C, Brice D A, Samimi P *et al*. *Annual Review of Materials Research*[J], 2016, 46: 63

3 Kumar P, Prakash O, Ramamurty U. *Acta Materialia*[J], 2018, 154: 246

4 Thijs L, Verhaeghe F, Craeghs T *et al*. *Acta Materialia*[J], 2010, 58(9): 3303

5 Saboori A, Gallo D, Biamino S *et al*. *Applied Sciences-Basel*[J], 2017, 7(9): 883

6 Amato K N, Gaytan S M, Murr L E *et al*. *Acta Materialia*[J], 2012, 60(5): 2229

7 Kruth J. *Journal of Materials Processing Tech*[J], 2004, 149(1-3): 616

8 Ding Y, Muniz-Lerma J A, Trask M *et al*. *MRS Bulletin*[J], 2016, 41(10): 745

9 Lewandowski J J, Seifi M. *Annual Review of Materials Research* [J], 2016, 46: 151

10 Murr L E, Gaytan S M, Ramirez D A *et al*. *Journal of Materials Science and Technology*[J], 2012, 28(1): 1

11 Niendorf T, Leuders S, Riemer A *et al*. *Metallurgical & Materials Transactions B*[J], 2013, 44(4): 794

12 Thijs L, Kempen K, Kruth J P *et al*. *Acta Materialia*[J], 2013, 61(5): 1809

13 Martin J H, Yahata B D, Hundley J M *et al*. *Nature*[J], 2017, 549(7672): 365

14 Chen Wei, Chen Chao, Zi Xuhui *et al*. *Materials Science & Engineering A*[J], 2018, 726: 240

15 Liu Min, Liu Shichao, Chen Wei *et al*. *Additive Manufacturing* [J], 2019, 30: 100 873

16 Niendorf T, Leuders S, Riemer A *et al*. *Advanced Engineering Materials*[J], 2014, 16(7): 857

17 Popovich V A, Borisov E V, Popovich A A *et al*. *Materials & Design*[J], 2016, 114: 441

18 Gaumann M, Henry S, Cleton F *et al*. *Materials Science & Engineering A*[J], 1999, 271(1-2): 232

19 Tan Xipeng, Kok Yihong, Tan Yujun *et al*. *Acta Materialia*[J], 2015, 97: 1

20 Wang Jian, Lin Xin, Wang Jitong *et al*. *Journal of Alloys and Compounds*[J], 2018, 768: 97

21 Sun S, Brandt M, Easton M. *Laser Additive Manufacturing*[J], 2017: 55

22 Wu X. *Material Science and Technology*[J], 2007, 23(6): 631

23 Yuan P, Gu D. *Journal of Physics D Applied Physics*[J], 2015, 48(3): 35 303

24 Harrison N J, Todd I, Mumtaz K. *Acta Materialia*[J], 2015, 94: 59

25 Loh L E, Chua C K, Yeong W Y *et al*. *International Journal of Heat & Mass Transfer*[J], 2015, 80: 288

26 Ahmed T, Rack H J. *Materials Science & Engineering A*[J], 1998, 243(1): 206

27 Lutjering G, Williams J C. *Titanium*[J], 2007: 345

28 Carroll B E, Palmer T A, Beese A M. *Acta Materialia*[J], 2015, 87: 309

29 Sanaei N, Fatemi A. *Progress in Materials Science*[J], 2020, 117: 100 724

利用选区激光熔化技术制备梯度结构的Ti-6Al-4V合金

刘世超[1,2]，雷鹏飞[3]，刘　敏[1,2]，张耕铭[1,2]，陈　超[1,2]，周科朝[1,2]

(1. 中南大学 粉末冶金研究院，湖南 长沙 410083)

(2. 中南大学 粉末冶金国家重点实验室，湖南 长沙 410083)

(3. 中南大学 湘雅医院 骨科，湖南 长沙 410083)

摘　要：采用选区激光熔化技术（SLM）制备了梯度Ti-6Al-4V合金。随着样品沉积厚度的逐渐增加，控制激光功率或扫描速率逐步升高或降低，以此研究了梯度结构Ti-6Al-4V合金的相变及结构演变。结果表明：由于选取激光熔化过程中的高冷却速率，SLM制备的Ti-6Al-4V合金的主要组织结构为初始β柱状晶里的针状马氏体。β柱状晶会随着激光功率的增加或扫描速率的降低而增宽。激光功率和扫描速率的变化会引起马氏体择优取向的变动。最后，由于局部不同的能量变化，随样品沉积厚度增加而逐步升高或降低的扫描速率会引发2种不同的空洞缺陷。

关键词：增材制造；选区激光熔化；Ti-6Al-4V；梯度结构；柱状晶

作者简介：刘世超，男，1990年生，博士后，中南大学粉末冶金研究院，湖南 长沙 410083，E-mail：pkhqchenchao@126.com